npj | breast cancer

Article

Published in partnership with the Breast Cancer Research Foundation

https://doi.org/10.1038/s41523-026-00910-7

Programmable local immunochemotherapy for triple-negative breast cancer via spatiotemporally controlled release of CpG oligodeoxynucleotides, gemcitabine, and paclitaxel

Cheng-Hsien Hsieh[1,2,15], Ming-Yi Hsu[3,4,15], Chiou-Feng Lin[1,5,6], Chien-Chun Liu[7,8], Yi-Hua Kuo[4], Yu-Ting Huang[9], Wei-Yu Chen[10,11], Shih-Jung Liu[4,12] ✉ & Wei-Jiunn Lee[1,13,14] ✉

Triple-negative breast cancer (TNBC) remains a highly aggressive subtype with limited targeted treatment options and substantial toxicity from systemic chemoimmunotherapy. We developed a Programmable Local Immunochemotherapy (PLICT) platform integrating a CpG oligodeoxynucleotide (CpG ODN)/gemcitabine-loaded hydrogel for rapid release and paclitaxel-loaded PLGA microspheres for sustained delivery. In a TNBC mouse model, peritumoral administration of PLICT enabled sequential release, facilitating the local delivery of immune agonist and chemotherapy to suppress early tumor growth, followed by prolonged inhibition of tumor progression and metastasis. Compared to systemic chemotherapy, PLICT significantly enhanced intratumoral cytotoxic T lymphocyte infiltration and favorably modulated the local immune microenvironment with minimal systemic toxicity. These findings highlight the therapeutic potential of PLICT as a locally administered, immune-potentiating strategy for effective TNBC treatment.

Triple-negative breast cancer (TNBC) is an aggressive breast cancer subtype that lacks expression of estrogen, progesterone, and HER2 receptors, which consequently limits the therapeutic options for targeted treatment[1,2]. TNBC exhibits significant intratumoral and intertumoral heterogeneity in terms of molecular subtypes, genomic alterations, and immune microenvironment characteristics. Currently, systemic chemotherapy, primarily utilizing cytotoxic agents such as anthracyclines and taxanes, remains the mainstay of treatment. However, TNBC exhibits high rates of recurrence and metastasis, coupled with significant intratumoral heterogeneity, posing significant clinical challenges and necessitating the development of novel therapeutic strategies that can effectively target TNBC while minimizing systemic toxicity and improving patient outcomes[3–5].

The immune environment within TNBC tumors is complex and generally characterized by a lower proportion of immune cells compared to

[1]Graduate Institute of Clinical Medicine, College of Medicine, Taipei Medical University, Taipei, Taiwan. [2]Department of Emergency Medicine, En Chu Kong Hospital, Sanxia, New Taipei City, Taiwan. [3]Department of Medical Imaging and Intervention, Chang Gung Memorial Hospital, Linkou, Taiwan. [4]Department of Mechanical Engineering, Chang Gung University, Taoyuan, Taiwan. [5]Department of Microbiology and Immunology, School of Medicine, College of Medicine, Taipei Medical University, Taipei, Taiwan. [6]Graduate Institute of Medical Sciences, Taipei Medical University, Taipei, Taiwan. [7]The School of Public Health and Medical Technology, Xiamen Medical College, Xiamen, Fujian, China. [8]Engineering Research Center of Natural Cosmeceuticals College of Fujian Province, Xiamen Medical College, Fujian, China. [9]Department of Diagnostic Radiology, Chang Gung Memorial Hospital, Keelung, Taiwan. [10]Department of Pathology, Wan Fang Hospital, Taipei Medical University, Taipei, Taiwan. [11]Department of Pathology, School of Medicine, College of Medicine, Taipei Medical University, Taipei, Taiwan. [12]Department of Orthopedic Surgery, Bone and Joint Research Center, Chang Gung Memorial Hospital, Taoyuan, Taiwan. [13]Department of Urology, School of Medicine, College of Medicine and TMU Research Center of Urology and Kidney (TMU-RCUK), Taipei Medical University, Taipei, Taiwan. [14]Department of Medical Education and Research, Wan Fang Hospital, Taipei Medical University, Taipei, Taiwan. [15]These authors contributed equally: Cheng-Hsien Hsieh, Ming-Yi Hsu. ✉e-mail: shihjung@mail.cgu.edu.tw; wjlee@tmu.edu.tw

other breast cancer subtypes[6–8]. However, TNBC can still attract tumor-infiltrating lymphocytes, including CD8+ cytotoxic T cells (CTLs), which are associated with better responses to treatment and improved prognosis[9–11]. Cancer immunotherapy, employing approaches such as immune checkpoint inhibitors and adoptive T cell transfer, marks a new era in cancer treatment by overcoming immune tolerance to tumor cells[12–15]. Recent clinical trials have demonstrated that incorporating pembrolizumab into neoadjuvant therapy results in improved therapeutic outcomes and extended survival in patients with TNBC[16–18]. However, this benefit appears to be limited to those exhibiting high levels of PD-L1 expression, suggesting that while immune checkpoint inhibitors may be an effective option for TNBC, their efficacy could vary among patients [18–20].

As a Toll-like receptor 9 (TLR9) agonist, CpG oligodeoxynucleotide (CpG ODN) is known to bolster anti-cancer immunity and establish long-term immunological memory[21,22]. Upon binding to TLR9, CpG ODN potently stimulates plasmacytoid dendritic cells to produce type I interferons, including IFN-α, thereby activating natural killer (NK) cells and CTLs and enhancing tumor cell recognition and elimination. CpG ODN are used as monotherapies or in combination with chemotherapy, radiation, or immune checkpoint inhibitors[22]. An unmet need in CpG ODN therapy lies in overcoming their susceptibility to nuclease degradation before they can be effectively recognized by antigen-presenting cells. Developing advanced delivery platforms that enhance drug stability and retention during treatment is crucial for achieving consistent immune activation and durable antitumor immunity.

For TNBC therapy, chemotherapy remains the primary non-surgical treatment. Common regimens involve anthracyclines, taxanes, or platinum-based drugs. Among taxanes, paclitaxel (PTX) is widely used. However, its low solubility necessitates the use of solvents or surfactants for administration, which can frequently cause hypersensitivity reactions. Our prior research demonstrated that PTX-loaded poly (lactic acid-*co*-glycolic acid) (PLGA) nanofibers could effectively deliver PTX without the need for solvents, thereby reducing systemic toxicity[23]. Additionally, the slow release mimicked the effects of metronomic chemotherapy, enhancing tumor suppression while minimizing side effects.

Recent clinical studies suggest that combining taxanes with other chemotherapeutic agents, such as gemcitabine (GEM), enhances therapeutic efficacy[23,24]. This improvement likely arises from their complementary mechanisms of action and differing toxicity profiles. However, the co-delivery of these agents in a single PLGA-based drug delivery system presents a significant challenge due to their differing solubility properties—GEM being hydrophilic and PTX hydrophobic. This incompatibility complicates the development of efficient delivery platforms that can simultaneously encapsulate and release both drugs effectively.

Electrospray technology is an advanced method that utilizes a high-voltage electric field to produce microspheres with consistent size and composition[25]. This process is ideal for encapsulating chemotherapeutic agents, as it allows tunable and reproducible control over particle size, morphology, and drug distribution. Microspheres generated through electrospraying can encapsulate one or more agents, protecting them from premature degradation and enabling the targeted, controlled release of the encapsulated agents.

Drug-loaded hydrogels are versatile, three-dimensional polymer networks that can hold and release therapeutic agents in a controlled and sustained manner[26]. Their hydrophilic structure enables high drug-loading efficiency and compatibility with a range of treatments, including chemotherapeutics, immunomodulators, and growth factors. When applied to cancer therapies, drug-loaded hydrogels can localize treatment directly to tumor sites, minimizing systemic toxicity. To enhance the bioavailability of CpG ODN and enable the co-delivery of GEM and PTX for tumor therapy, we developed a novel programmable local immunochemotherapy (PLICT) platform. This platform incorporates PTX-loaded electrosprayed microspheres within a GEM and CpG ODN hydrogel. By leveraging local delivery, PLICT is designed to release CpG ODN, GEM, and PTX sequentially, mimicking metronomic chemotherapy while potentiating immune activation.

Results

Fabrication and morphological characterization of PTX-loaded electrosprayed microspheres

PTX-loaded microspheres were fabricated using the electrospray technique, as schematically illustrated in Fig. 1a. The process was carried out under controlled environmental conditions (22–24 °C, 44–49% relative humidity), where a polymer-to-drug ratio of 5:3 (PLGA: PTX) was used for fabrication. The surface morphology of the microspheres is shown in Fig. 1b and c, revealing a predominantly spherical morphology with a smooth surface. Based on SEM image analysis using ImageJ software, the average particle size was determined to be 10.16 ± 2.98 μm, with the size distribution histogram shown in Fig. 1d. The surface charge of the microspheres was evaluated using the electrophoretic light scattering (ELS) technique, yielding a zeta potential of 1.36 ± 0.2 mV. Although a polydispersity index (PDI) of 1.806 was recorded via dynamic light scattering (DLS), this high value was primarily attributed to the microscale dimensions of the particles (~10 μm), which exceed the optimal range for Brownian motion-based DLS analysis. Given that the microspheres are dominated by gravitational sedimentation rather than Brownian diffusion, the SEM-derived size and distribution were utilized as the primary indicators of particle uniformity and quality.

The FTIR spectra of PTX-loaded PLGA microparticles and GEM-embedded hydrogel

After being incorporated into the PLGA matrix, all characteristic vibration peaks of PTX could still be observed, demonstrating the structural integrity of the drug (Fig. 2a). In addition, the new vibration peak at 1650 cm^{-1} is attributed to the N–H bonds in PTX. The C–H vibration at 900 cm^{-1} was enhanced owing to the addition of the drug, while the new peak at 720 cm^{-1} was due to the C–O bond of the incorporated PTX. Similarly, Fig. 2b presents the FTIR spectra of gemcitabine, PF-127, and gemcitabine-loaded PF-127. All major vibrations of gemcitabine appeared in the gemcitabine/PF-127 mixture, confirming the integrity of the drug. Furthermore, the vibrations at 3200, 1745, and 1400 cm^{-1} resulted from the O–H, C = O, and C–F bonds, respectively, of the incorporated gemcitabine. These findings confirm the successful incorporation of PTX and gemcitabine into the microparticles and hydrogel.

In Vitro drug release profile of PTX-loaded electrosprayed microspheres

The in vitro release profile of PTX from the PTX-loaded electrosprayed microspheres was evaluated over a 30-day period (Fig. 3). Samples were collected at regular intervals to monitor the cumulative release of PTX. Throughout the study, PTX demonstrated a stable, sustained release without any detectable initial burst. At the conclusion of the 30-day period, the total cumulative release of PTX reached 62.1% of the encapsulated drug, indicating an efficient and controlled release mechanism of the microspheres.

PLICT enhances tumor suppression in orthotopic TNBC mouse model

To evaluate the therapeutic efficacy of PLICT in controlling TNBC growth and metastasis, 6-week-old female BALB/c mice were orthotopically inoculated with 3×10^5 luciferase-expressing murine 4T1 mammary tumor cells in the fourth mammary fat pads (Fig. 4). Seven days post-inoculation, mice were randomly assigned to one of four treatment groups: (1) Vehicle control, (2) PTX (i.p.), (3) PTX + GEM (i.p.), and (4) PLICT, as detailed in the materials and methods section. At the conclusion of the study, tumors were surgically excised from the mice. After carefully removing any residual microspheres from the tumor tissue, a portion of the tumor was subjected to flow cytometry for immune cell profiling, while another portion was processed for residual PTX concentration analysis.

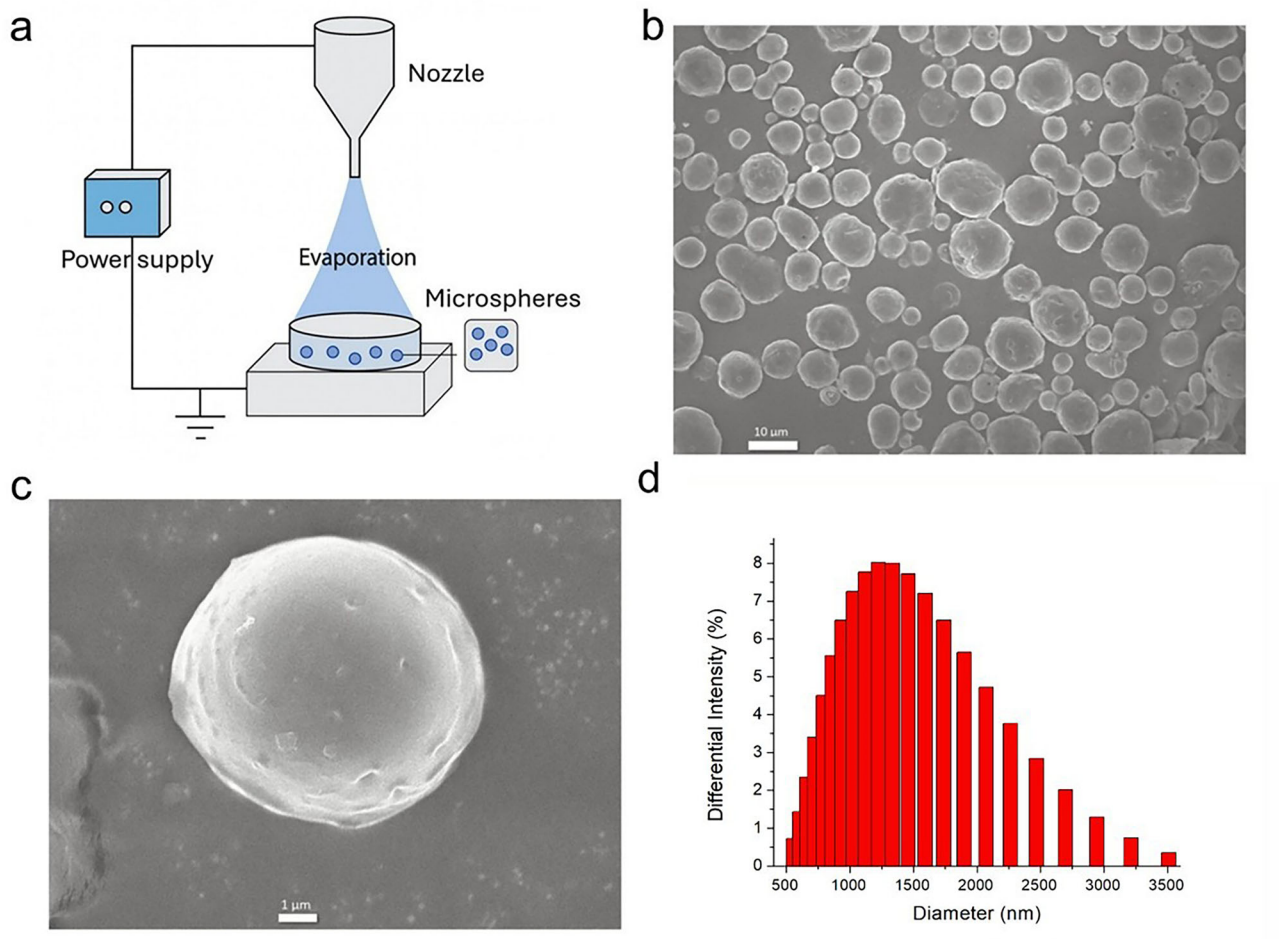

Fig. 1 | Fabrication and morphological characterization of PTX-loaded electrosprayed microspheres. a Schematic diagram of the electrospray setup for the fabrication of microspheres. **b**, **c** SEM image showing the surface morphology of PTX-loaded PLGA microspheres. **d** Diameter distribution of PTX-loaded PLGA microspheres.

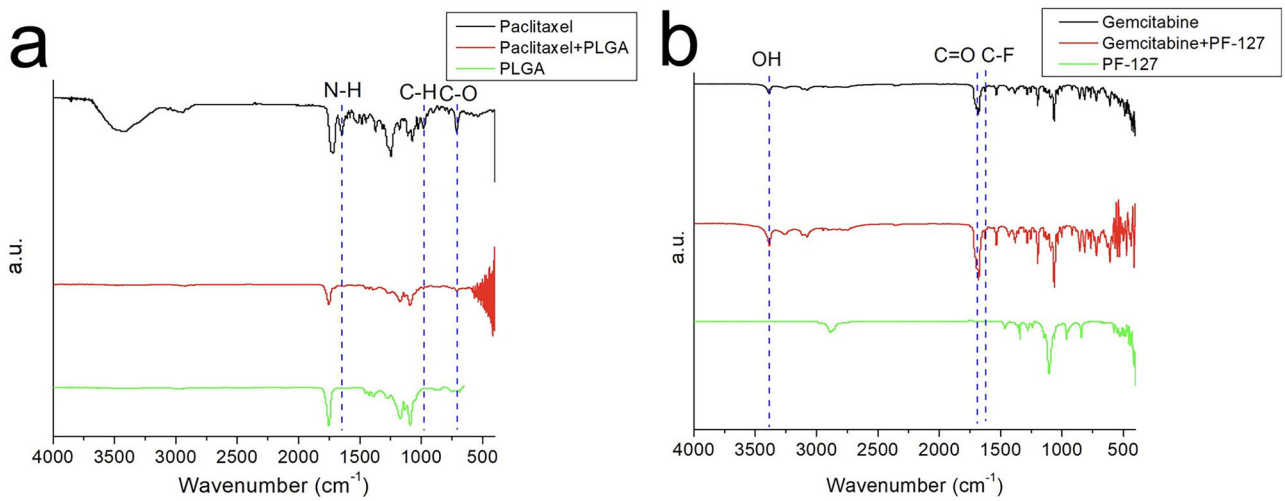

Fig. 2 | Fourier-transform spectra. a PTX-loaded mircoparticles, **b** gemcitabine-embedded hydrogel.

Mice were subjected to the specific treatment regimens as outlined in the experimental design. Tumor growth showed a clear and distinct pattern across the treatment groups, with the vehicle group displaying the most rapid progression of tumor growth (Fig. 5). The PTX i.p. group exhibited a noticeable reduction in tumor size compared to the vehicle group, followed by the PTX + GEM i.p. group, which demonstrated further inhibition of tumor progression. However, the most significant suppression of tumor growth was observed in the PLICT group, where tumor expansion was drastically reduced. These results highlight the superior efficacy of PLICT in controlling tumor growth compared to other treatment modalities.

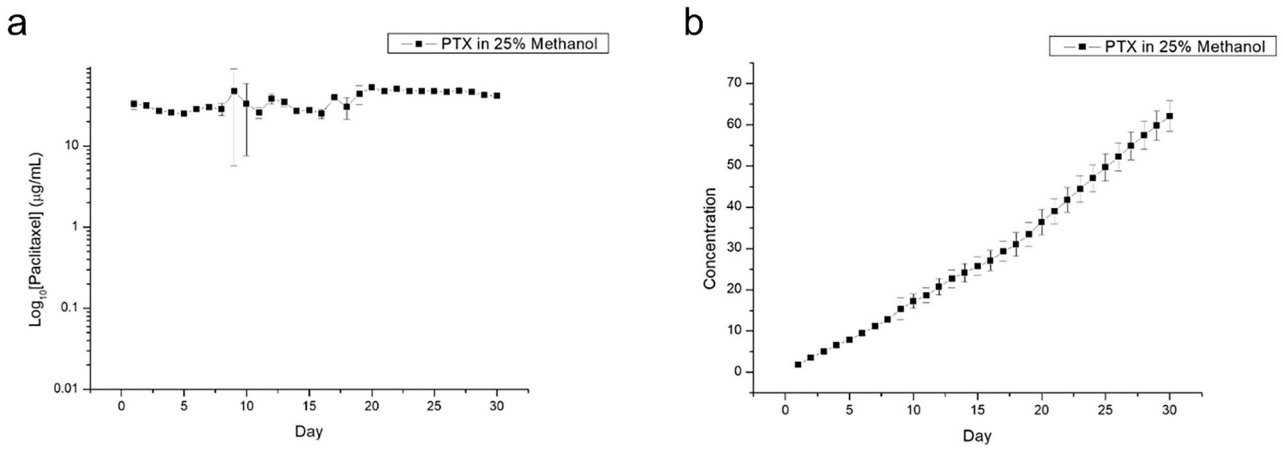

Fig. 3 | In vitro release profile of PTX from PTX-loaded electrosprayed microspheres. Samples were collected at regular intervals, and the daily release (**a**) and cumulative release (**b**) of PTX was quantified. Data are expressed as the mean ± SD of triplicate measurements.

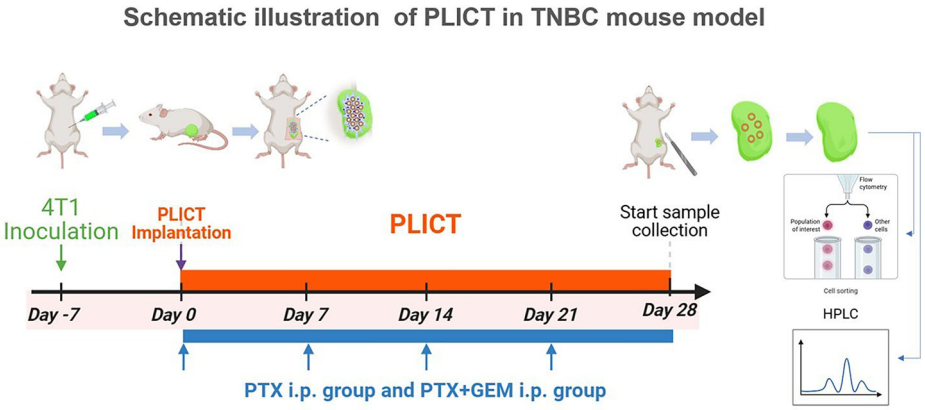

Fig. 4 | Schematic representation of the experimental design and treatment protocol. The top part of the figure shows a schematic representation of the mammary gland transplantation procedure. On Day -7, 4T1-Luc tumor cells were inoculated into the 4th mammary fat pads of 6-week-old female BALB/c mice. On day 0, a 5-mm incision was made in the mammary gland epithelium of mice in PLICT group to transplant PLICT into the fat pad. Mice in the PTX i.p. and PTX + GEM i.p. groups received correlated chemotherapy weekly for four consecutive weeks. Tumor size and growth were monitored weekly by bioluminescent imaging. On Day 28, tumors were excised and any remaining microspheres were carefully removed. The tumor tissues were then analyzed for immune cell profiles via flow cytometry and for residual PTX concentration.

PLICT reduces metastasis in orthotopic TNBC mouse model

To further assess metastatic potential, ex vivo BLI was performed on dissected organs 28 days post-tumor implantation. Significant differences were observed among groups in bioluminescence signal intensity, tumor volume, and tumor weight (Fig. 6a–c). Consistent with these findings, the vehicle group exhibited the highest metastatic burden, followed by the PTX i.p. and PTX + GEM i.p. groups. Notably, the PLICT group demonstrated the most substantial reduction in metastatic spread, as evidenced by significantly lower bioluminescence signals in metastatic organs (Fig. 6d). These differences underscore the enhanced therapeutic effect of PLICT, which outperformed the other treatments in reducing both tumor size and bioluminescent signals, confirming its potent antitumor activity.

PLICT promotes the expansion of cytotoxic T lymphocytes within the tumor microenvironment

Building on the prior findings of enhanced tumor growth inhibition, we investigated whether PLICT's potent antitumor effects in TNBC might also modify the immune cell composition within the tumor microenvironment. Flow cytometry was performed on resected 4T1 tumors after PLICT treatment to identify shifts in immune cell profiles and understand the potential mechanisms underlying PLICT's therapeutic effects. Initial analysis focused on the overall T-cell population within the tumor microenvironment. While the PLICT group exhibited a trend towards increased T-cell infiltration compared to the vehicle, PTX i.p., and PTX + GEM i.p. groups, this difference did not reach statistical significance (Fig. 7a). However, a notable increase in the proportion of Tc cells was observed exclusively in PLICT-treated tumors, highlighting the treatment's specific impact on this critical subset of T cells ($p < 0.01$, Fig. 7b). This increase in Tc cells (11.27%), coupled with the lack of a similar response in other treatment groups (vehicle group: 1.92%, PTX i.p. group: 2.43%, PTX + GEM i.p. group: 2.30%), suggests that PLICT may particularly enhance the tumor-killing capacity by enriching the CTLs population. The PLICT group also demonstrated a modest increase in regulatory Tc cells compared to the Vehicle group ($p < 0.05$, Fig. 7c), which was far outweighed by the robust expansion of cytotoxic T cells. Moreover, while the helper T-cell population remained relatively consistent across all treatment conditions (Fig. 7d), a decrease in regulatory helper T cells was observed in the PLICT group compared to the vehicle group (Fig. 7e). Interestingly, regulatory helper T cells, which are typically associated with immune suppression within tumors, were significantly reduced in PLICT-treated tumors compared to other groups. This reduction may imply a beneficial shift toward modulated immune microenvironment that could further support antitumor immunity and potentiate the efficacy of CTLs within the tumor site.

In terms of innate immune cells, we observed that NKs were most prevalent in tumors of the PTX i.p. group (Fig. 7f). This finding emphasizes that while the PTX i.p. group may bolster certain aspects of the innate immune response, PLICT's effect is more pronounced within the adaptive immune system, particularly affecting CTLs.

Collectively, these results indicate that PLICT favorably modulates the intratumoral immune microenvironment, characterized by increased CTLs and a reduction in suppressive regulatory helper T cells. This unique immune modulation by PLICT could be instrumental in its observed tumor-suppressive effects, offering promising insights into its potential as a targeted immunochemotherapy for TNBC.

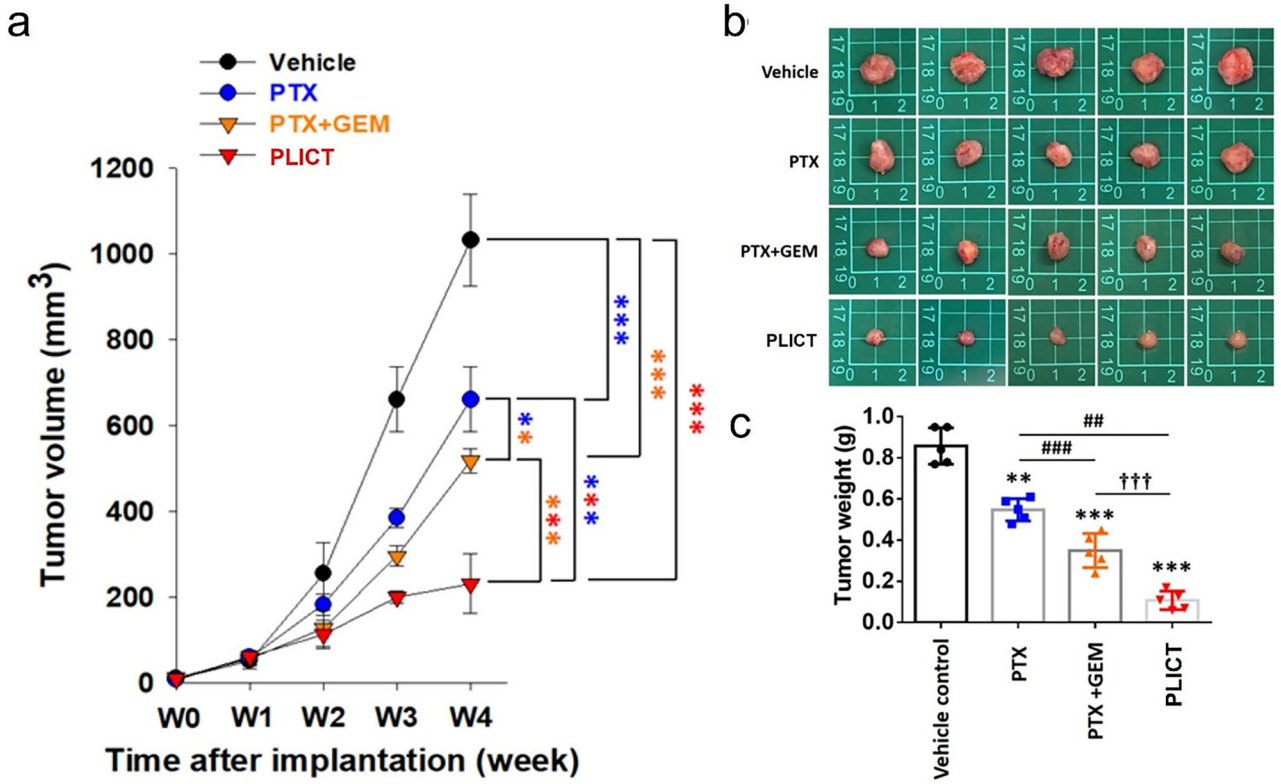

Fig. 5 | PLICT enhanced antitumor efficacy in the orthotopic TNBC Mouse Model. **a** Tumor growth curve. The volumes of 4T1-Luc tumors were measured and calculated using the following formula: volume = width^2 × length × 0.5236. Data are presented as tumor volumes in each group (n = 5 tumors/group). **b** Representative images of tumors excised from mice after 28 days of treatment. **c** The mean tumor weight of each group at the study endpoint. Data are expressed as mean ± SD. $^{*}p < 0.05$, $^{**/\#\#}p < 0.01$, $^{***/\#\#\#/\dagger\dagger\dagger}p < 0.001$.

PLICT enhances intratumoral accumulation of PTX and reduces off-target effects

To understand how PLICT treatment influences intratumoral PTX concentration and its distribution in surrounding tissue, we analyzed PTX levels in the tumors and contralateral fat pads. Following PLICT treatment, tumors showed a significantly higher PTX concentration compared to PTX i.p. and PTX + GEM i.p. groups ($p < 0.05$, Fig. 8a), indicating that PLICT enables enhanced PTX retention within the tumor microenvironment. Meanwhile, there were no significant differences in blood PTX levels among the groups (Fig. 8b). In contrast, PTX levels in the contralateral fat pad were notably lower in the PLICT group, exhibiting a significant reduction ($p < 0.001$, Fig. 8c). This differential distribution pattern highlights PLICT's targeted delivery capabilities, concentrating therapeutic effects within the tumor while minimizing off-target effects.

Functional validation of antitumor immunity via CD69 activation

While the increased ratio of CTLs in the PLICT-treated tumors was observed in our flow cytometric analysis (Fig. 7), it remained unknown whether the complex interplay between the sustained release of the immunoadjuvant (CpG ODN) and the cytotoxic agents successfully led to the functional activation of these infiltrating cells. To assess the immune activation status in situ, we performed immunohistochemical (IHC) staining for CD69, a well-established early T-cell activation marker. Analysis of the tumor sections revealed a marked upregulation of the CD69 marker, demonstrating a significantly higher enumeration of activated CD69$^+$ T cells in the PLICT treatment group compared to all control and monotherapy groups (Fig. 9). This observation, coupled with the original finding of enhanced CTL infiltration, confirms that the CpG ODN released from the PLICT platform maintained its biological potency and successfully engaged the TLR9 signaling pathway. Collectively, the robust increase in both the number of CTLs and their activation status (CD69$^+$) provides compelling functional evidence that the released immunoadjuvant successfully orchestrated a productive adaptive immune response, synergizing with the chemotherapeutics to achieve the observed superior tumor control and therapeutic efficacy.

Assessment of systemic toxicity of PLITC

To evaluate the potential systemic toxicity of PLICT treatment, liver, kidney, brain, and lung tissues were collected from mice for histological sectioning and hematoxylin–eosin (H&E) staining to assess tissue morphology and the in vivo safety profile of PLICT (Fig. 10). H&E staining revealed normal hepatic architecture and hepatocyte morphology in the vehicle group. In contrast, mice treated with systemic chemotherapy (PTX i.p. or PTX + GEM i.p.) exhibited hepatocellular swelling, marked sinusoidal compression, and prominent inflammatory cell infiltration. Notably, the PLICT group demonstrated substantially attenuated histopathological damage, closely resembling the vehicle group. Furthermore, no notable histological damage or inflammatory infiltration was observed in the glomeruli, renal tubules, neurons, or pulmonary epithelial cells across any treatment group. Collectively, these findings indicate that PLICT not only confers superior therapeutic efficacy but is also associated with markedly reduced systemic toxicity and a favorable in vivo safety profile.

Discussion

The highly heterogeneous nature of TNBC and the paucity of effective therapeutic options beyond chemotherapy have contributed to its notoriously poor prognosis. Emerging research has highlighted the concept of tumor-immune co-evolution, whereby metastatic tumors evolve mechanisms to evade immune surveillance, resulting in significant phenotypic and genotypic differences compared to their primary counterparts. This evolutionary process highlights the importance of considering metastatic TNBC as a complex ecosystem, characterized by both intrinsic and extrinsic

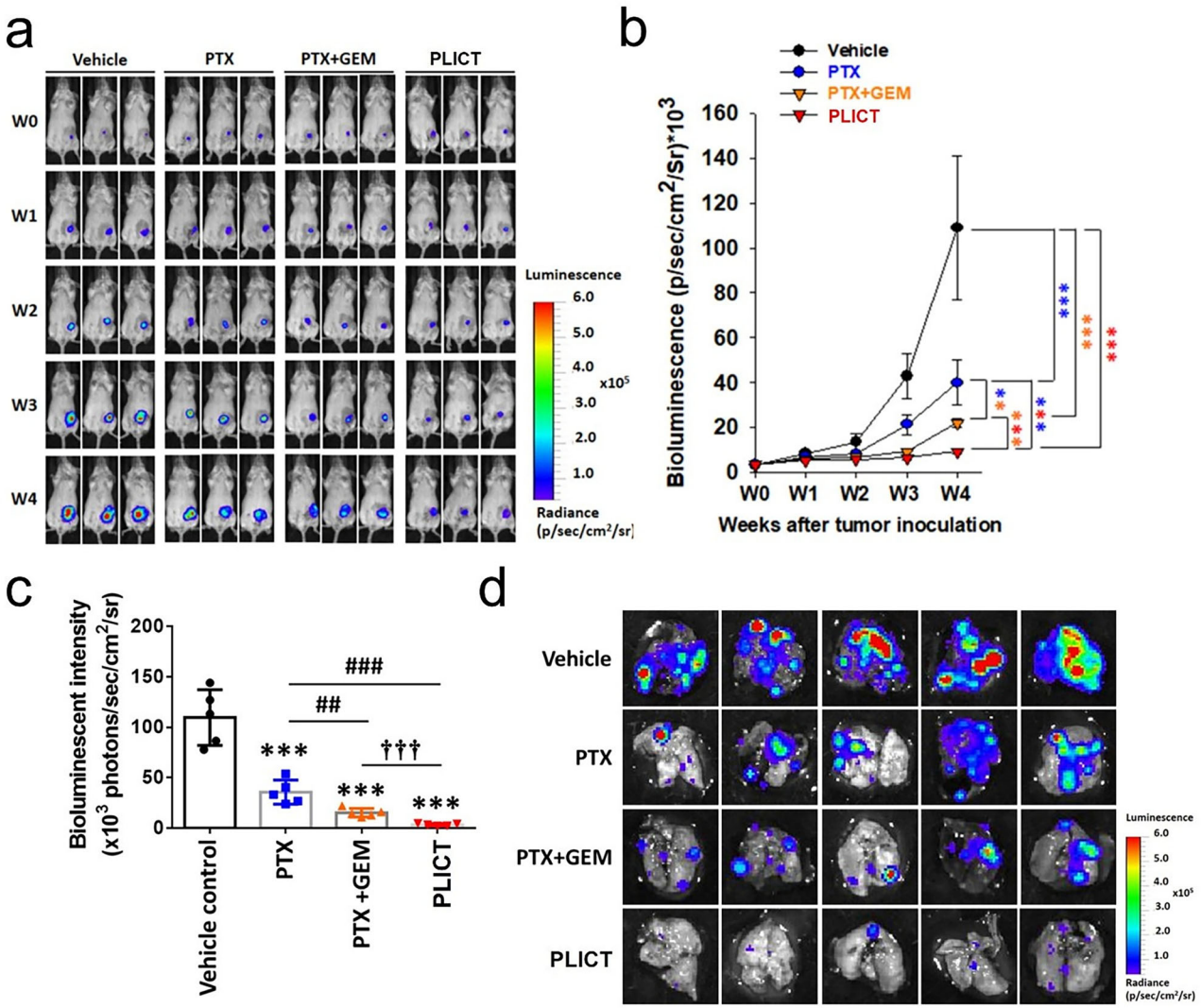

Fig. 6 | Inhibition of tumor growth and metastasis by PLICT in an orthotopic TNBC mouse model. a Mice were euthanized and dissected on day 28, with representative non-invasive bioluminescent imaging (BLI) of tumor-bearing mice performed at specified intervals using the IVIS system. **b** Quantitative assessment of Xenogen imaging signal intensity (photons/s) was conducted at designated time points. **c** Representative ex vivo BLI of metastatic sites in the 4T1-Luc orthotopic breast cancer spontaneous metastasis model; lungs were excised and imaged at study termination, with mean signal intensity reported for each group. **d** Signal intensity analysis at the experiment's conclusion. Data are presented as mean ± SD. $^{*}p < 0.05$, $^{**}/\#\#p < 0.01$, $^{***}/\#\#\#/\dagger\dagger\dagger p < 0.001$.

factors that contribute to its aggressive nature[27]. Notably, post-treatment metastases exhibit a higher frequency of private "driver" mutations, suggesting that therapeutic interventions promote clonal selection and evolution[28]. Moreover, metastatic sites exhibit a pronounced immunodepleted state, characterized by reduced numbers of tumor-infiltrating lymphocytes, CTLs, and dendritic cells, alongside diminished expression of immunomodulatory genes, such as interferon-related signatures[27,29,30]. Therefore, developing strategies to suppress TNBC growth while promoting intratumoral immunity and preventing metastatic dissemination is imperative.

Our study demonstrates that PLICT offers a significant advantage over conventional injectable chemotherapy for treating TNBC. The sequential release of GEM and CpG ODN, followed by sustained delivery of PTX, represents a novel therapeutic strategy for TNBC. Initially, the release of GEM from the hydrogel reduces tumor burden, providing an immediate cytotoxic effect. Concurrently, CpG ODN is released, modulating immune responses within the tumor microenvironment and enhancing the presence of CTLs. Finally, PTX is released from the microspheres, providing sustained tumor growth inhibition over time. PLICT achieves superior tumor growth inhibition and reduces metastatic spread while minimizing systemic exposure to chemotherapeutic agents in non-target tissues. Additionally, PLICT enhances the proportion of CTLs within the tumor microenvironment, suggesting modulation of the immune microenvironment. These findings underscore the potential of PLICT as a more effective and localized therapeutic approach, offering a dual benefit of direct tumor suppression and immune modulation.

Metronomic chemotherapy (MCT) is a therapeutic strategy involving the sustained administration of low-dose chemotherapeutics. Its mechanisms of action include direct tumor suppression, disruption of angiogenesis within the tumor microenvironment, and stimulation of intratumoral immune activation[31,32]. Previous investigations from our laboratory have indicated that local delivery of PTX, analogous to metronomic chemotherapy, exerts inhibitory effects on tumor growth and angiogenesis[23]. While single-drug MCT has shown moderate efficacy, combining two chemotherapeutics can yield enhanced outcomes[33]. Emerging evidence also supports combining MCT with immune checkpoint inhibitors for enhanced anti-tumor effects[32]. However, in clinical practice, MCT is often restricted to palliative care in late-stage cancer due to practical constraints, such as reliance on oral chemotherapeutic agents for patient convenience. In this study, we present PLICT as a next-generation approach that mirrors the

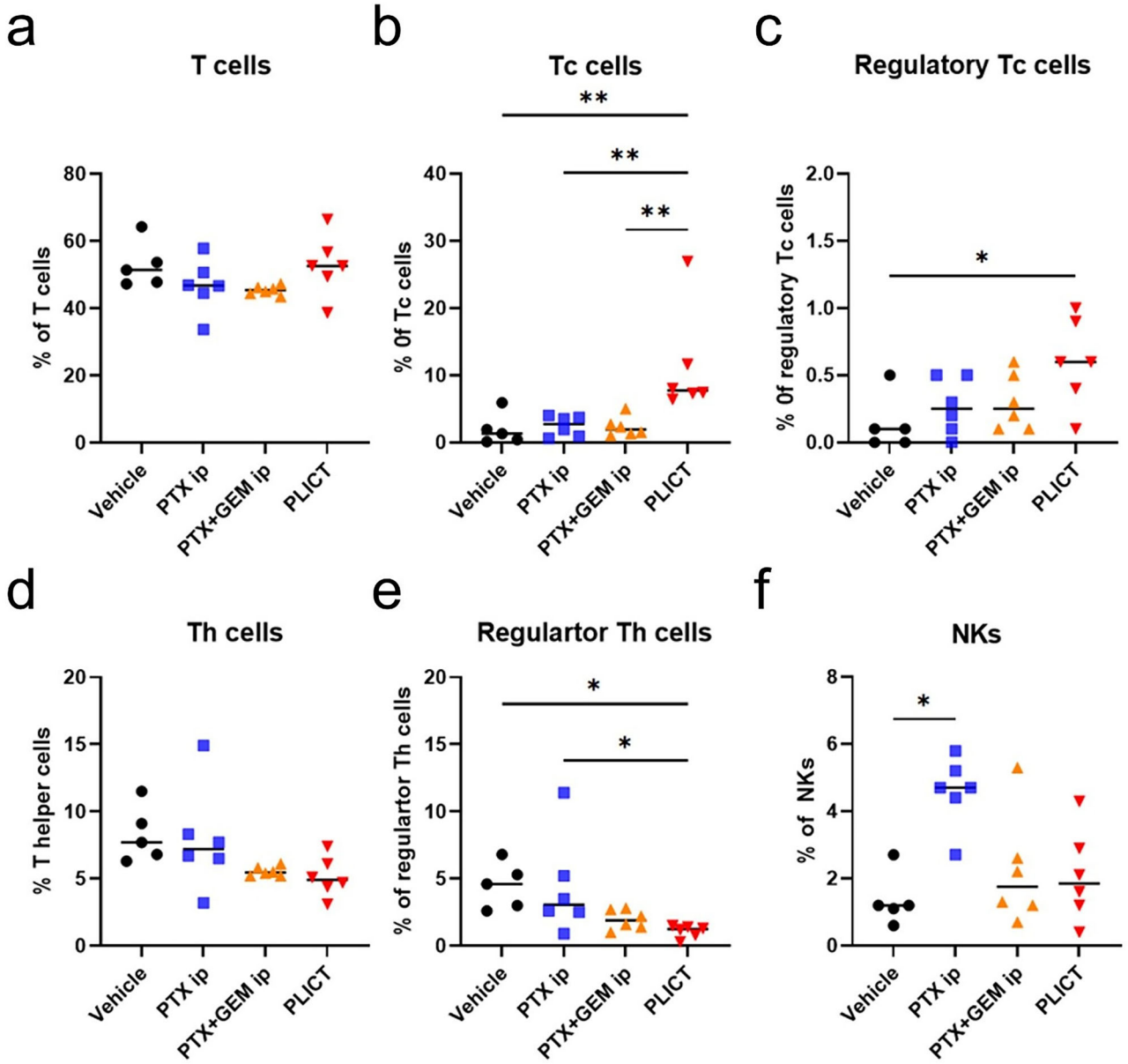

Fig. 7 | Intratumoral immune cell profiles in TNBC tumors after PLICT treatment. a Flow cytometric analysis of total T cells within the tumor microenvironment. Quantification of CD8+ T cells (**b**) and regulatory CD8+ T cells (**c**) within the tumor microenvironment. Analysis of CD4+ (**d**) and CD25+FoxP3+ regulatory T cells (**e**) within the tumor microenvironment. **f** Analysis of NK cells within the tumor microenvironment. Data are presented as mean ± SD. $^{*}p < 0.05$, $^{**}p < 0.01$, compared to the vehicle group.

benefits of MCT while overcoming its limitations. By providing continuous, long-lasting, and stable drug release, PLICT achieves high intratumoral drug concentrations, minimal systemic toxicity, reduced distant metastasis, and robust immune activation without requiring drug-free intervals. Moreover, PLICT offers the versatility to incorporate non-oral chemotherapeutic agents, deliver combinations of drugs with differing solubility profiles, and precisely tailor release sequences to maximize therapeutic outcomes. It utilizes a thermosensitive hydrogel to carry hydrophilic drugs and hydrophobic drug-coated PLGA microspheres, enabling administration via fine needles. The 5–15 μm size range (averaging 10.16 ± 2.98 μm) was selected to balance biological retention with deliverability. Diameters >5 μm minimize macrophage-mediated clearance[34,35], while ensuring smooth administration through 26–30 G needles without clogging. Furthermore, the observed polydispersity facilitates a multi-phased release where smaller particles provide early-stage release contribution and larger ones ensure sustained delivery, directly supporting the goals of our PLICT strategy. This minimally invasive option allows for imaging-guided techniques to safely and effectively deliver therapeutic agents to various parts of the body for cancer treatment. From a clinical perspective, PLICT requires only a single injection to provide long-term drug release, eliminating the need for surgical interventions or prolonged intravenous injections. This not only enhances patient comfort but also improves treatment compliance, offering a highly practical and efficient alternative for cancer therapy.

The literature has increasingly acknowledged the efficacy of TLR9 agonizts as an adjuvant in mitigating the immunosuppressive effects of myeloid-derived suppressor cells and promoting immune infiltration, particularly in tumors with low immunogenicity[21,22]. However, the short in vivo half-life of CpG ODN due to degradation by nucleases has limited their clinical application. We hypothesized that the sustained-release properties of PLICT offer a promising strategy to prolong the in vivo retention time of CpG ODN, thereby enhancing immune stimulation. Flow cytometric analysis was conducted to quantify immune cell subsets within the tumor microenvironment. In accordance with our prediction, PLICT treatment increased the proportion of intratumoral CTLs. Our findings further

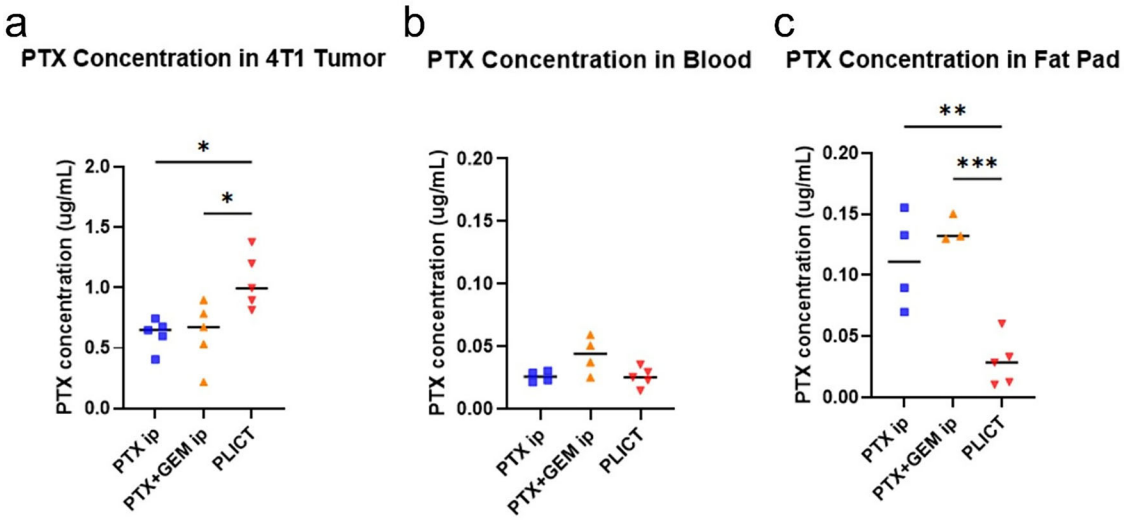

Fig. 8 | Quantitative analysis of PTX concentration in TNBC tumors and peripheral fat pad following PLICT treatment. a PTX concentration in tumors. **b** PTX concentration in blood. **c** PTX concentration in the peripheral fat pad. Data are expressed as mean ± SD. $^{*}p < 0.05$, $^{**}p < 0.01$, $^{***}p < 0.001$.

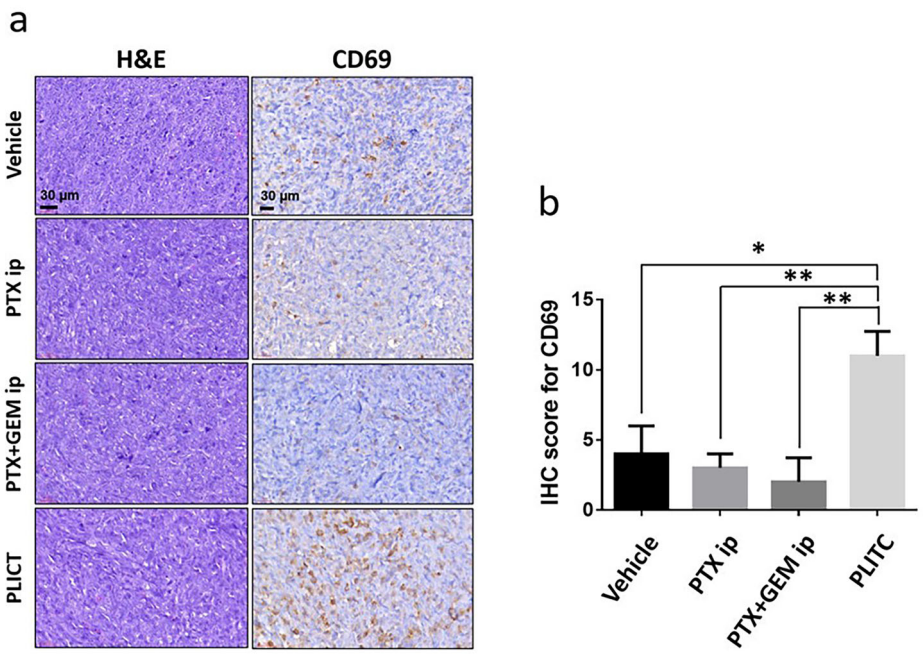

Fig. 9 | Immunohistochemical analysis of T-cell activation status (CD69) in the tumor microenvironment. a Representative Images of tumor sections for H&E and CD69. Tumor sections from mice following various treatments (Control, PTX i.p., PTX + GEM i.p., and PLICT) were stained for CD69 to assess the activation status of tumor-infiltrating T cells. Cell nuclei are counterstained with Hematoxylin (blue). (Scale bar: 30 μm; Original magnification: ×400). **b** Quantification of Activated T Cells. IHC staining scores for CD69 expression were compared among the different tumor treatment groups. CD69 expression was significantly higher in the PLITC-treated group. Data are presented as mean ± SD. $^{*}p < 0.05$, $^{**}p < 0.01$, $^{***}p < 0.001$.

corroborate the notion from previous studies that the extent of tumor infiltration by CTLs is positively correlated with prognosis[36–41]. Intriguingly, while previous studies have demonstrated that CpG ODN treatment can increase monocytes and tumor-infiltrating lymphocytes, the PLICT treatment in our study did not yield the same results[37–39]. Those studies typically involved multiple administrations of CpG ODN throughout the experiment, whereas PLICT consisted of CpG ODN release at the beginning. This discrepancy may be attributed to differences in experimental design. However, the exact reasons underlying this difference require further investigation.

Distant metastasis, the spread of cancer cells from the primary site to distant organs, is the primary cause of cancer-related deaths and limits the efficacy of surgery. A prerequisite for successful metastasis is the formation of pre-metastatic niches in distant organs, which are specialized microenvironments that facilitate the colonization and growth of tumor cells[42,43]. Pre-metastatic niches are induced by factors secreted by primary tumors and are characterized by alterations in the microenvironment of distant organs, including increased vascular permeability, immune suppression, and remodeling of the extracellular matrix. Chemotherapy, while effective in eliminating primary tumors, can inadvertently promote metastasis[44–46]. By damaging both the primary tumor and distant organs, chemotherapy can induce the release of circulating tumor cells and tumor-associated factors that further enhance pre-metastatic niche formation and impair antitumor immune responses. PLICT offers a promising therapeutic approach by delivering high concentrations of chemotherapeutic agents locally to the primary tumor, thereby minimizing off-target effects on distant organs. The MCT-mimicking effect of local PTX delivery may also reduce angiogenesis in the tumor microenvironment[23]. Furthermore, PLICT demonstrated an increase in the infiltration of tumor-infiltrating T cells within the tumor, leading to a more robust antitumor immune response. Consequently, by targeting the primary tumor and reducing systemic drug exposure, PLICT may mitigate the formation of pre-metastatic niches in distant organs, thereby reducing the potential for metastasis compared to systemic chemotherapy.

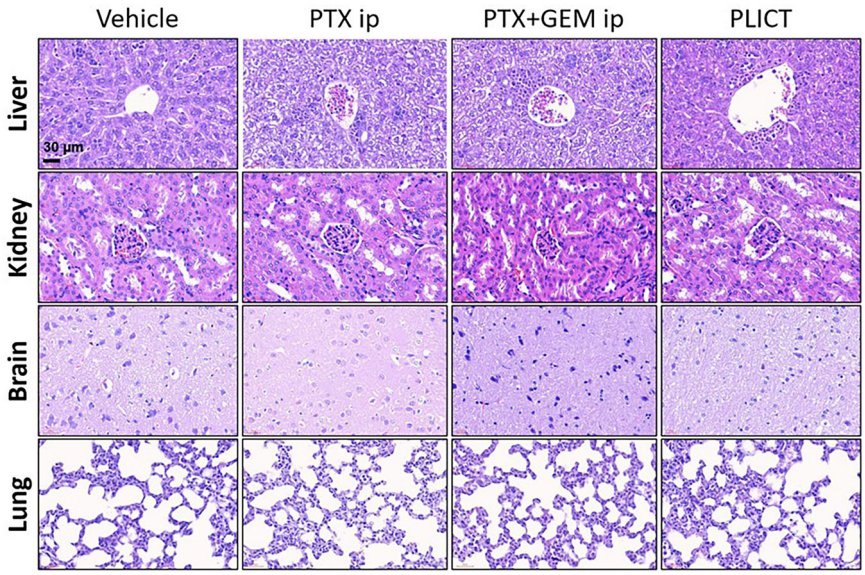

Fig. 10 | Histopathological analysis (Hematoxylin and Eosin staining) of major organs (×400). Histological sections of the major organs (liver, kidney, brain, and lung) collected from mice in the vehicle, PTX i.p., PTX + GEM i.p., or PLICT groups were stained with hematoxylin and eosin (H&E) for pathological analysis. Representative images were acquired at ×400 magnification. All scale bars represent 30 μm.

This study has several limitations. First, while intravenous injection is a standard route of administration, PTX and GEM were delivered via intraperitoneal injection in this study. Second, the efficacy of PLICT in patients with metastatic disease, post-surgical recurrence, or as a neoadjuvant therapy remains unclear and requires further investigation. Third, the current immune profiling is limited to cell population frequencies and activation, which only partially addresses the complex balance of immune activation in the tumor microenvironment. Furthermore, the tumor specificity of the enhanced CTL response has not been confirmed. Future work, including ex vivo assays using tumor lysates to stimulate memory T cells, is essential to definitively characterize the quality and durability of the PLICT-induced immune response. However, it is anticipated that PLICT could effectively control the local recurrence of the tumor.

There remains ample room for further investigation into the PLICT platform. For instance, the platform has the potential to integrate a variety of drugs with disparate properties, such as incompatible chemotherapeutic agents, immune checkpoint inhibitors, targeted therapy, tumor vaccines, mRNA-based cancer therapeutics, and antibody-based immunotherapy, to achieve maximal synergistic effects. Moreover, by leveraging the varying half-lives of different drug carriers, it is feasible to sequentially release three or more distinct regimens within a single platform at various time points. Additionally, as this study only released CpG ODN at the initial stage of the experiment, intermittent release could be explored to identify the optimal dosing interval and dosage, thereby maximizing the body's immune system's ability to eliminate tumor cells. Crucially, it is intuitively inferred that the therapeutic efficacy of PLICT, being a local delivery platform, would be significantly limited or unsuitable for widespread hematologic malignancies (e.g., leukemia) that lack a defined solid tumor mass. Lastly, developing specific PLICT platforms for different tumor types and integrating PLICT with surgery and radiation therapy could potentially lead to optimal control or even a cure.

In conclusion, this study demonstrates the significant potential of PLICT as a novel therapeutic approach for triple-negative breast cancer. By combining the cytotoxic effects of GEM, the immunostimulatory properties of CpG ODN, and the sustained release of paclitaxel, PLICT effectively inhibits tumor growth, reduces metastatic burden, and enhances intratumoral immunity. The sequential release of these therapeutic agents within a single platform offers a more precise and personalized approach to cancer treatment, addressing the limitations of traditional systemic chemotherapy. Moreover, PLICT's ability to mimic metronomic chemotherapy while avoiding systemic side effects provides a compelling rationale for its clinical translation. Future studies should investigate the efficacy of PLICT in combination with other therapeutic modalities, such as immune checkpoint inhibitors, and explore its application in various tumor types. Overall, our findings suggest that PLICT represents a promising strategy for improving the treatment of triple-negative breast cancer.

Methods

Reagents

PLGA (Resomer RG 503, Boehringer, Rhein Ingelheim, Germany; lactide: glycolide ratio 50:50, MW 33,000 Da) was used for microsphere fabrication. PTX, GEM, PF-127 hydrogel, Dimethyl sulfoxide (DMSO), and Dichloromethane (DCM) were purchased from Sigma-Aldrich Co. (St. Louis, MO, USA). Electrospraying was performed using an apparatus consisting of a needle and syringe, an aluminum collection plate, a grounding electrode, and a high-voltage direct current (DC) power supply. CpG ODNs were synthesized by Sangon Biotech (Shanghai, China) according to sequences reported in the literature[47]. Fetal bovine serum, penicillin-streptomycin, trypsin-EDTA, and trypan blue were purchased from Life Technologies (Gaithersburg, MD, USA). An enhanced chemiluminescence kit was obtained from Amersham (Arlington Heights, IL, USA). All other cell culture reagents were of standard laboratory grade.

Cell lines and cell culture

The murine 4T1 TNBC cells, obtained from the American Type Culture Collection (ATCC, Rockville, MD, USA), were cultured in RPMI 1640 GlutaMAX™ medium (Gibco™, Thermo Fisher Scientific, Waltham, MA, USA) and supplemented with 10% fetal bovine serum (FBS) (HyClone, GE Healthcare, Chicago, IL, USA), 1 mM sodium pyruvate, and 3.5 g/L glucose (Sigma-Aldrich, Saint Louis, MO, USA).

Preparation and manufacturing of PTX-loaded electrosprayed microspheres

PTX-loaded microspheres were fabricated using the electrospray technique based on previous studies[48]. A total of 150 mg PLGA and 90 mg PTX were added to 3 mL of a mixture of DCM with the drug loading of 37.5 wt%. This solution was loaded into a 2.5 mL glass syringe equipped with a 26-gauge stainless steel needle (Terumo, Tokyo, Japan, and Becton Dickinson, Franklin Lakes, NJ, USA). Electrospraying was performed under controlled environmental conditions (22–24 °C, 44–49% relative humidity). The polymer solution was extruded through the needle at a constant flow rate of 0.3 mL/h using a syringe pump (World Precision Instruments, Sarasota, FL, USA) towards a grounded aluminum foil collector (20 × 20 cm^2) positioned 12 cm from the needle tip. A high voltage of 12 kV was applied between the

needle and the collector. Following electrospraying, the collected microspheres were placed in a vacuum chamber for 72 h to remove any residual solvent. Subsequently, the microspheres were transferred to glass vials and further evacuated for storage.

Preparation and manufacturing of GEM and CpG ODN DNA hydrogel

Pleuronic F-127 powder was hydrated in distilled water at 4 °C to form a hydrogel (20% w/v). A drug-loaded hydrogel was prepared by adding 1.2 mg/mL GEM and 0.2 mg/mL CpG ODN to the hydrated PF-127 solution. This yields a CpG ODN loading capacity of approximately 0.1 wt%. The hydrogel was stored at 4 °C until further use.

Characterization of PTX-loaded microspheres and gemcitabine-embedded hydrogel

To characterize the surface morphology of the PTX-loaded electrosprayed microspheres, they were gold-coated and subsequently imaged using a scanning electron microscope (SEM; S3000N; Hitachi, Tokyo, Japan). The zeta potential and polydispersity index (PDI) were analyzed by an ELSZ-2000 particle size analyzer (Otsuka Electronics, Osaka, Japan).

Spectral characterization of the drug-loaded microparticles and hydrogels was performed using a Thermo-Fisher Nicolet iS5 FTIR spectrometer (Waltham, MA, USA). The instrument operated at a resolution of 4 cm^{-1} with 32 scans. Samples were pressed into KBr discs, and spectra were obtained across the 500–4000 cm^{-1} range.

In vitro drug release study

In vitro drug release studies were conducted using a modified sink condition. Briefly, PTX from electrosprayed microsphere samples was incubated in 1 mL of dissolution medium (phosphate-buffered saline (PBS), pH 7.4, containing 25% methanol) at 37 °C. At 24-h intervals, the release medium was collected and replaced with fresh medium. PTX concentrations in the collected samples were determined using high-performance liquid chromatography (HPLC). The HPLC analysis was performed with Hitachi HPLC liquid chromatograph system comprised Hitachi CM 5160 pump, Hitachi CM 5310 column oven, Hitachi CM5260 Auto Sampler: and Hitachi CM 5420 UV-VIS detector. The column used for separation of the PTX was a Waters SunFire ® C18 5 µm 4.6 x 250 mm. The mobile phase contained deionized water and acetonitrile (50:50 v/v). The absorbency was monitored at 227 nm, and the flow rate was 1.0 mL/min with a retention time of 20 min and pressure of 230 mmHg. PTX was detected at 227 nm. A standard curve was generated using known concentrations of PTX ($R^2 = 0.9997$), demonstrating excellent linearity for accurate quantification. Each release study was performed in triplicate for 30 days to ensure reproducibility.

Orthotopic 4T1 TNBC mouse model

Female BALB/c mice (6 weeks old) were procured from the National Laboratory Animal Center (Taipei, Taiwan). All animal procedures were conducted in compliance with institutional guidelines and approved by the Institutional Animal Care and Use Committee (IACUC). To establish an orthotopic model of triple-negative breast cancer (TNBC), mice were anesthetized with 3% isoflurane delivered via a precision vaporizer system, ensuring consistent depth of anesthesia throughout the procedure. Using a 27-gauge needle, 5×10^5 4T1 cells stably expressing green fluorescent protein (GFP) and firefly luciferase were suspended in a 1:1 ratio of phosphate-buffered saline (PBS) and growth factor-reduced Matrigel and injected into the right inguinal mammary fat pad. Following tumor cell inoculation, mice were monitored daily for general health and tumor engraftment. After a 7-day tumor establishment period, tumor burden was evaluated by bioluminescent imaging (BLI) using the Xenogen IVIS Spectrum system. Mice exhibiting comparable BLI signals were randomly assigned into four experimental groups, ensuring balanced tumor volumes at baseline to minimize inter-group variability in subsequent analyses. The experimental groups were: Group 1 (Vehicle control): topical application of a blank hydrogel combined with unloaded PLGA microspheres directly onto the tumor surface. Group 2 (PTX): Weekly intraperitoneal (i.p.) administration of paclitaxel (PTX) at a dose of 10 mg/kg (equivalent to 0.2 mg/mouse) formulated in 10% DMSO, for a total duration of 4 weeks. Group 3 (PTX + GEM): Intraperitoneal administration of a combination of PTX (10 mg/kg) and gemcitabine (GEM, 60 mg/kg; equivalent to 1.2 mg/mouse) during the first week, followed by PTX alone (10 mg/kg) once weekly for the subsequent 3 weeks. Group 4 (PLICT): Local application of 500 µL of the PLICT formulation directly onto the tumor surface, containing 0.8 mg/mouse PTX, 1.2 mg/mouse GEM, and 100 µg/mouse CpG oligodeoxynucleotide (CpG ODN).

Evaluation of antitumor activity

To evaluate antitumor efficacy, twenty female BALB/c mice were randomly allocated into four experimental groups ($n = 5$ per group). Tumor progression was monitored weekly using in vivo bioluminescence imaging (BLI) with the IVIS Imaging System (Caliper Life Sciences, Alameda, CA, USA). Tumor dimensions were measured weekly with calipers, and tumor volumes were calculated accordingly. On day 28, all mice were euthanized, and ex vivo BLI of the excised tumor-bearing tissues was performed using the IVIS Spectrum system. Tumor weights were measured at the time of tissue collection.

Bioluminescence image

Mice were anesthetized with 1–3% isoflurane and subsequently placed into the IVIS imaging system (Xenogen). Each animal received an intraperitoneal injection of 100 µL of d-luciferin (30 mg/mL; Caliper Life Sciences). Bioluminescent acquisition was initiated approximately 2 min after substrate delivery. During the treatment period, metastatic burden was evaluated longitudinally by serial imaging. The initial acquisition time was set at 2 min, with subsequent exposures adjusted based on signal intensity to avoid saturation. Image analysis was conducted using Living Image software (Xenogen). Regions of interest (ROIs) were drawn over the entire animal or specific organs to quantify the bioluminescent signal, expressed as photon flux (photons/s/cm^2).

Flow cytometry analysis

To analyze the immune cell composition within the tumor microenvironment (TME) of 4T1 tumor-bearing mice, the mice were euthanized, and tumors were carefully excised. Tumor tissues were mechanically disrupted using a Tenbroeck (Corning) homogenizer in DMEM supplemented with 10% FBS. Tumor-infiltrating immune cells were enriched by density gradient centrifugation using 30/70% Percoll (GE Lifesciences). Isolated cells were resuspended in PBS containing 2% FBS and incubated with anti-CD16/CD32 to block non-specific antibody binding. For flow cytometry analysis, cells were stained with the following antibody panels: All T cells: CD3+; Cytotoxic T cells (Tc): CD3+ CD8+; Helper T cells (Th): CD3+ CD4+; Regulatory T cells: CD3+ CD4+ CD25+ FoxP3+; NK cells: CD3− CD56+; NKT cells: CD3+ CD56+; CD4+ NKT cells: CD3+ CD4+ CD56+; CD8+ NKT cells: CD3+ CD8+ CD56+; Macrophages: CD45+ F4/80+; M1 macrophages: CD45+ F4/80+ CD86+; M2 macrophages: CD45+ F4/80+ CD209+. All staining procedures were performed at 4 °C for 30 min, followed by three washes with flow buffer between each step (live/dead staining, blocking, surface staining, intracellular staining). Flow cytometry data were acquired using a FACSAria flow cytometer (BD Biosciences) and analyzed with FlowJo software (version 10, Tree Star Software).

Sample preparation and HPLC analysis

At the conclusion of the in vivo study, tissue samples from the experimental mice were collected for further analysis of PTX concentration. Methanol with 0.1% (v/v) acetic acid was used as the solvent for tissue extraction to prevent rapid degradation of PTX. The tissue samples were homogenized in 3 mL of methanol at a speed of 6 m/s for 30 s using a homogenizer

(Prep-CB24, MedClub, Taoyuan, Taiwan). This process was repeated three times to ensure thorough extraction. Following homogenization, the samples were filtered through a polyvinylidene difluoride syringe filter (0.22-μm pore size). After centrifugation at 10,000 rpm for 10 min, the supernatant was collected and injected into the HPLC system for quantification and further analysis.

Haematoxylin and Eosin (H&E) staining

Formalin-fixed, paraffin-embedded tissue sections were deparaffinized in xylene and rehydrated through a graded ethanol series to distilled water. Sections were then stained with hematoxylin for 5 min, followed by rinsing in running tap water for 5 min to achieve bluing. Counterstaining was performed with eosin for 30 s. Subsequently, sections were dehydrated through a graded ethanol series, cleared in xylene, and mounted with neutral resin mounting medium. Representative microscopic fields were captured for imaging.

Immunohistochemical (IHC) staining

Mouse tumor tissues were fixed in 10% (v/v) neutral buffered formalin, paraffin-embedded, and sectioned at a thickness of 3 μm. Sections were deparaffinized in xylene and rehydrated through a graded ethanol series to distilled water. Antigen retrieval was performed by heating sections in 0.1 M citrate buffer (pH 6.0) using a microwave oven. Endogenous peroxidase activity was quenched with hydrogen peroxide, followed by blocking with normal serum to reduce non-specific binding. Sections were then incubated overnight at 4 °C with a primary antibody against CD69 (1:500; ab322534, Abcam). Immunoreactivity was visualized using the Dako REAL EnVision Detection System (Agilent Technologies, Santa Clara, CA, USA), with hematoxylin used as a nuclear counterstain. Stained sections were digitally scanned using the Motic EasyScan system (Motic, Hong Kong, China). Representative images were acquired for analysis.

Semiquantitative IHC scoring

The semiquantitative IHC score for CD69 was determined based on a combination of staining intensity and the percentage of positively stained cells. Staining intensity was graded according to DAB color intensity as follows: 0, negative; 1, weak; 2, moderate; and 3, strong. The percentage of positively stained cells was scored as: 0 (<5%), 1 (5–24%), 2 (25–49%), 3 (50–74%), and 4 (75–100%). The final IHC score was calculated by multiplying the intensity score by the percentage score.

Ethics statement

All animal experiments were approved by the Institutional Animal Care and Use Committee (IACUC) of Taipei Medical University (IACUC Approval No.: WAN-LAC-110-021). The protocol of the animal study on mice was based on the guidelines provided by the Council for International Organizations of Medical Sciences (CIOMS). Female BALB/c mice (6–8 weeks old, the National Laboratory Animal Center of Taiwan) were used, with efforts to minimize animal suffering, including anesthesia during peritumoral injections and humane endpoints for tumor burden.

Clinical trial number: not applicable. This study was conducted using an orthotopic TNBC mouse model and did not involve human clinical trials.

Statistical analysis

Statistical analyses were performed using SPSS Statistics software (version 12.0; IBM Corp., Armonk, NY, USA). Paired sample t-tests were employed to compare data between groups. Data are presented as mean ± standard deviation. Statistical significance was defined as $p < 0.05$.

Data availability

The datasets generated and analyzed during the current study are available from the corresponding author upon reasonable request. Data access is subject to the formalization of a Data Transfer Agreement and must ensure full compliance with the Personal Data Protection Act of Taiwan.

Received: 14 September 2025; Accepted: 30 January 2026;
Published online: 13 February 2026

References

1. Zagami, P. & Carey, L. A. Triple negative breast cancer: pitfalls and progress. *NPJ Breast Cancer* **8**, 95 (2022).
2. Zerdan, M. B. et al. Triple negative breast cancer: updates on classification and treatment in 2021. *Cancers* **14**, 1253 (2022).
3. Li, X. et al. Triple-negative breast cancer has worse overall survival and cause-specific survival than non-triple-negative breast cancer. *Breast Cancer Res. Treat.* **161**, 279–287 (2017).
4. Hsu, J. Y., Chang, C. J. & Cheng, J. S. Survival, treatment regimens and medical costs of women newly diagnosed with metastatic triple-negative breast cancer. *Sci. Rep.* **12**, 729 (2022).
5. Obidiro, O., Battogtokh, G. & Akala, E.O. Triple negative breast cancer treatment options and limitations: future outlook, *Pharmaceutics* **15**, 1796 (2023).
6. Fan, Y. & He, S. The characteristics of tumor microenvironment in triple negative breast cancer. *Cancer Manag. Res.* **14**, 1–17 (2022).
7. So, J. Y., Ohm, J., Lipkowitz, S. & Yang, L. Triple negative breast cancer (TNBC): non-genetic tumor heterogeneity and immune microenvironment: Emerging treatment options. *Pharm. Ther.* **237**, 108253 (2022).
8. Harris, M. A. et al. Towards targeting the breast cancer immune microenvironment. *Nat. Rev. Cancer* **24**, 554–577 (2024).
9. de Moraes, F. C. A., Souza, M. E. C., Sano, V. K. T., Moraes, R. A. & Melo, A. C. Association of tumor-infiltrating lymphocytes with clinical outcomes in patients with triple-negative breast cancer receiving neoadjuvant chemotherapy: a systematic review and meta-analysis. *Clin. Transl. Oncol.* **27**, 974–987 (2024).
10. Leon-Ferre, R.A. & International Immuno-Oncology Biomarker Working Group. Tumor-infiltrating lymphocytes in triple-negative breast cancer. JAMA **331**, 1135–1144 (2024).
11. Gao, G., Wang, Z., Qu, X. & Zhang, Z. Prognostic value of tumor-infiltrating lymphocytes in patients with triple-negative breast cancer: a systematic review and meta-analysis. *BMC Cancer* **20**, 179 (2020).
12. Luo, C. et al. Progress and prospect of immunotherapy for triple-negative breast cancer. *Front. Oncol.* **12**, 919072 (2022).
13. Zhu, Y., Zhu, X., Tang, C., Guan, X. & Zhang, W. Progress and challenges of immunotherapy in triple-negative breast cancer. *Biochim. Biophys. Acta Rev. Cancer* **1876**, 188593 (2021).
14. Shewale, H. & Kanugo, A. Recent advances in immunotherapy and targeted therapy of triple negative breast cancer. *Curr. Pharm. Biotechnol.* **26**, 365–391 (2024).
15. Liu, Y. et al. Advances in immunotherapy for triple-negative breast cancer. *Mol. Cancer* **22**, 145 (2023).
16. Tarantino, P., Gandini, S., Trapani, D., Criscitiello, C. & Curigliano, G. Immunotherapy addition to neoadjuvant chemotherapy for early triple negative breast cancer: a systematic review and meta-analysis of randomized clinical trials. *Crit. Rev. Oncol. Hematol.* **159**, 103223 (2021).
17. Huo, X. et al. Addition of immunotherapy to chemotherapy for metastatic triple-negative breast cancer: a systematic review and meta-analysis of randomized clinical trials. *Crit. Rev. Oncol. Hematol.* **168**, 103530 (2021).
18. Howard, F. M., Pearson, A. T. & Nanda, R. Clinical trials of immunotherapy in triple-negative breast cancer. *Breast Cancer Res. Treat.* **195**, 1–15 (2022).
19. Mittendorf, E. A. et al. Neoadjuvant atezolizumab in combination with sequential nab-paclitaxel and anthracycline-based chemotherapy versus placebo and chemotherapy in patients with early-stage triple-negative breast cancer (IMpassion031): a randomised, double-blind, phase 3 trial. *Lancet* **396**, 1090–1100 (2020).
20. Schmid, P., Dent, R. & O'Shaughnessy, J. Pembrolizumab for early triple-negative breast cancer. *N. Engl. J. Med.* **382**, e108 (2020).

21. Chen, W. et al. CpG-based nanovaccines for cancer immunotherapy. *Int. J. Nanomed.* **16**, 5281–5299 (2021).
22. Rolfo, C., Giovannetti, E., Martinez, P., McCue, S. & Naing, A. Applications and clinical trial landscape using Toll-like receptor agonists to reduce the toll of cancer. *NPJ Precis. Oncol.* **7**, 26 (2023).
23. Hsu, M. Y. et al. Enhanced paclitaxel efficacy to suppress triple-negative breast cancer progression using metronomic chemotherapy with a controlled release system of electrospun poly-d-l-lactide-co-glycolide (PLGA) nanofibers. *Cancers* **13**, 3350 (2021).
24. Hu, Q. et al. A systematic review of gemcitabine and taxanes combination therapy randomized trials for metastatic breast cancer. *SpringerPlus* **3**, 293 (2014).
25. Alfatama, M., Shahzad, Y. & Choukaife, H. Recent advances of electrospray technique for multiparticulate preparation: drug delivery applications. *Adv. Colloid Interface Sci.* **325**, 103098 (2024).
26. Vigata, M., Meinert, C., Hutmacher, D. W. & Bock, N. Hydrogels as drug delivery systems: a review of current characterization and evaluation techniques. *Pharmaceutics* **12**, 1188 (2020).
27. Bianchini, G., De Angelis, C., Licata, L. & Gianni, L. Treatment landscape of triple-negative breast cancer - expanded options, evolving needs. *Nat. Rev. Clin. Oncol.* **19**, 91–113 (2022).
28. Bertucci, F. et al. Genomic characterization of metastatic breast cancers. *Nature* **569**, 560–564 (2019).
29. Zhu, L. et al. Metastatic breast cancers have reduced immune cell recruitment but harbor increased macrophages relative to their matched primary tumors. *J. Immunother. Cancer* **7**, 265 (2019).
30. Hutchinson, K. E. et al. Comprehensive profiling of poor-risk paired primary and recurrent triple-negative breast cancers reveals immune phenotype shifts. *Clin. Cancer Res.* **26**, 657–668 (2020).
31. Cazzaniga, M.E. et al. Metronomic chemotherapy. *Cancers* **13**, 2236 (2021).
32. Muraro, E. et al. Metronomic chemotherapy: anti-tumor pathways and combination with immune checkpoint inhibitors. *Cancers* **15** (2023).
33. Varayathu, H., Sarathy, V., Thomas, B. E., Mufti, S. S. & Naik, R. Combination strategies to augment immune check point inhibitors efficacy - implications for translational research. *Front. Oncol.* **11**, 559161 (2021).
34. Tabata, Y. & Ikada, Y. Effect of the size and surface charge of polymer microspheres on their phagocytosis by macrophage. *Biomaterials* **9**, 356–62 (1988).
35. Sarmadi, M. et al. Modeling, design, and machine learning-based framework for optimal injectability of microparticle-based drug formulations. *Sci. Adv.* **6**, eabb6594 (2020).
36. Su, C. et al. Enhancing radiotherapy response via intratumoral injection of a TLR9 agonist in autochthonous murine sarcomas. *JCI Insight*. **9**, e178767 (2024).
37. Dongye, Z. et al. Icaritin and intratumoral injection of CpG treatment synergistically promote T cell infiltration and antitumor immune response in mice. *Int. Immunopharmacol.* **111**, 109093 (2022).
38. Liu, J. et al. Programmable delivery of immune adjuvant to tumor-infiltrating dendritic cells for cancer immunotherapy. *Nano Lett.* **20**, 4882–4889 (2020).
39. Kadiyala, P. et al. High-density lipoprotein-mimicking nanodiscs for chemo-immunotherapy against glioblastoma multiforme. *ACS Nano* **13**, 1365–1384 (2019).
40. Shirota, Y., Shirota, H. & Klinman, D. M. Intratumoral injection of CpG oligonucleotides induces the differentiation and reduces the immunosuppressive activity of myeloid-derived suppressor cells. *J. Immunol.* **188**, 1592–9 (2012).
41. Ali, H. R. et al. Association between CD8+ T-cell infiltration and breast cancer survival in 12,439 patients. *Ann. Oncol.* **25**, 1536–43 (2014).
42. Patras, L., Shaashua, L., Matei, I. & Lyden, D. Immune determinants of the pre-metastatic niche. *Cancer Cell* **41**, 546–572 (2023).
43. Wang, Y. et al. Pre-metastatic niche: formation, characteristics and therapeutic implication. *Signal Transduct. Target Ther.* **9**, 236 (2024).
44. Keklikoglou, I. et al. Chemotherapy elicits pro-metastatic extracellular vesicles in breast cancer models. *Nat. Cell Biol.* **21**, 190–202 (2019).
45. Monteran, L. et al. Chemotherapy-induced complement signaling modulates immunosuppression and metastatic relapse in breast cancer. *Nat. Commun.* **13**, 5797 (2022).
46. Karagiannis, G. S., Condeelis, J. S. & Oktay, M. H. Chemotherapy-induced metastasis: mechanisms and translational opportunities. *Clin. Exp. Metastasis* **35**, 269–284 (2018).
47. Nishikawa, M. et al. Biodegradable CpG DNA hydrogels for sustained delivery of doxorubicin and immunostimulatory signals in tumor-bearing mice. *Biomaterials* **32**, 488–94 (2011).
48. Hsu, M. Y. et al. Preparation and in vitro/in vivo evaluation of doxorubicin-loaded poly[lactic-co-glycol acid] microspheres using electrospray method for sustained drug delivery and potential intratumoral injection. *Colloids Surf. B Biointerfaces* **190**, 110937 (2020).

Acknowledgements

No specific acknowledgements are required for this study. This work was supported by Chang Gung Memorial Hospital, Taiwan [grant number: CMRPG2N0011] to M.Y. Hsu, by National Natural Science Foundation of China [grant number: 82502675] to C.C. Liu; by Natural Science Foundation of Fujian Province, Fujian, China [grant 2025J011475 to C.-C. Liu], by the fund of the Educational Research Project for Young and Middle-aged Teachers in Fujian Province [grant number: JZ240078 to C.C. Liu] and Wan Fang Hospital, Taiwan [grant number:112-wf-eva-06] to W.J. Lee. These funders had no role in study design, data collection and analysis, decision to publish, or preparation of the manuscript.

Author contributions

C.H. Hsieh and M.Y. Hsu jointly conceived the study and designed the research framework. C.F. Lin conducted flow cytometry experiments and analyzed the related data. C.C. Liu oversaw the synthesis and preparation of CpG oligodeoxynucleotides. Y.H. Kuo performed the fabrication of electrosprayed microspheres. W.Y. Chen contributed the pathological assessment and interpretation of the H&E and CD69 immunohistochemistry data. W.J. Li managed animal-related experiments and collected the corresponding data. C.H. Hsieh, M.Y. Hsu and Y.T. Huang drafted the initial manuscript. C.F. Lin, S.J. Liu, and W.J. Li reviewed and edited the manuscript for intellectual content.

Competing interests

The authors declare no competing interests.

Additional information

Supplementary information The online version contains supplementary material available at https://doi.org/10.1038/s41523-026-00910-7.

Correspondence and requests for materials should be addressed to Shih-Jung Liu or Wei-Jiunn Lee.